

Emulating dynamic non-linear simulators using Gaussian processes

Hossein Mohammadi ^{*1,2}, Peter Challenor ^{†1,2}, and Marc Goodfellow ^{‡1,2}

¹College of Engineering, Mathematics and Physical Sciences, University of Exeter,
Exeter, UK

²EPSRC Centre for Predictive Modelling in Healthcare, University of Exeter, Exeter,
UK

Abstract

In this paper, we examine the emulation of non-linear deterministic computer codes where the output is a time series, possibly multivariate. Such computer models simulate the evolution of some real-world phenomena over time, for example models of the climate or the functioning of the human brain. The models we are interested in are highly non-linear and exhibit tipping points, bifurcations and chaotic behaviour. However, each simulation run could be too time-consuming to perform analyses that require many runs, including quantifying the variation in model output with respect to changes in the inputs. We therefore build emulators using Gaussian processes to approximate the output of the code. We use the Gaussian process to predict one-step ahead in an iterative way over the whole time series. We consider a number of ways to propagate uncertainty through the time series including both the uncertainty of inputs to the emulators at time t and the correlation between them. The methodology is illustrated with a number of examples. These include the highly non-linear dynamical systems described by the Lorenz and Van der Pol equations. In both cases we will show that we not only have very good predictive performance but also have measures of uncertainty that reflect what is known about predictability in each system.

Keywords: Dynamic emulators, Gaussian processes, Uncertainty propagation, Lorenz, Van der Pol.

1 Introduction

Computer models, e.g. numerical simulators, are sophisticated mathematical representations of some real-world phenomena implemented in computer programs [37]. Such models are widely

*Corresponding Author: h.mohammadi@exeter.ac.uk

†p.g.challenor@exeter.ac.uk

‡m.goodfellow@exeter.ac.uk

used in many fields of science and technology to aid our understanding of physical processes or because conducting physical experiments is too costly, highly time-consuming or even impossible in some cases [47]. In some cases, simulators are available as commercial packages and the underlying functions are unknown to the user. In most applications, it is crucial to understand the sensitivity of model outputs to variation or uncertainty in inputs [37]. Performing such quantitative studies require a large number of simulation runs, see for example [12]. It becomes impractical if each simulation run is time-consuming.

Emulators, also known as *surrogate models*, *metamodels* or *response surfaces* [24] provide a “fast” approximation of complex simulation models using a limited number of training runs. The most popular classes of emulators are neural networks, splines, regression models, etc. We refer the reader to [17, 7, 13] for more information on different types of emulators and their properties. Among the diverse types of emulators, Gaussian processes (GPs) have become increasingly popular over the last two decades in the field of the design and analysis of computer experiments [47, 48, 19]. Also known as Kriging, especially in geostatistics [10], GPs have been effectively used in many real-world applications including wireless communication [49], metallurgy [2], biology [54, 21, 28], environmental science [29, 6], and sensor placements [25].

There are several reasons for the popularity of GPs. Firstly, they can be used to fit any smooth (with different degrees of smoothness), continuous function thanks to the variety of covariance kernels available [36]. See Sect. 2 for more details on kernels. Secondly, GPs are non-parametric models, i.e., no strong assumptions about the form of the underlying function are required, unlike polynomial regression [42]. Moreover, the prediction performance of GPs is comparable to (if not better than) other methods such as neural networks [40, 22], the limit of a single layer neural network as the number of neurons tends to infinity is a Gaussian process [33, 35]. The main advantage of GPs is that they provide not only a mean predictor but also a quantification of the associated uncertainty. This uncertainty reflects the prediction accuracy and can serve as a criterion to enhance prediction capability of the emulator [18].

This paper deals with the emulation of dynamic computer models that simulate phenomena evolving with time. The output of a dynamic simulator is a time series for each input. The time series represents the change in the model state variables from one time step to the next. Such models are often expressed by a system of differential equations.

Dynamic simulators appear in many applications. For instance, Stommel’s box model [52] simulates the evolution of temperature and salinity to determine the ocean density. In [4] a dynamic model is developed whose output is a time series of general practice consultations for the 2009 A/H1N1 influenza epidemic in London. Since this model is computationally expensive, a GP emulator is developed for calibration [11]. Another real-world example of dynamic computer models is presented in [26] where a saturated path hydrology model simulates the movement of water at catchment scales. In [56] large climate models with time series output that exhibit chaotic behaviour are emulated using Bayesian dynamic linear model Gaussian processes. We refer to [9] for more examples on such simulators.

2 Gaussian processes as emulators

Let f be the underlying function of an expensive simulator we want to approximate (or predict) defined as $f: \mathcal{X} \mapsto \mathcal{F}$. Here, $\mathcal{X} \subset \mathbb{R}^d$ and $\mathcal{F} \subset \mathbb{R}^q$ are the input and output space respectively. We further assume that f is a “black-box” function; there is no analytic expression for it and additional information such as gradients are not available. Also throughout this paper we assume the simulator to be *deterministic* (vs. *stochastic*); i.e. if it is run twice with same inputs, the outputs will be identical.

A GP defines a distribution over functions which can be regarded as a generalisation of the normal distribution to infinite dimensions. Formally, a GP indexed by \mathcal{X} is a collection of random variables $\{Z_{\mathbf{x}}, \mathbf{x} \in \mathcal{X}\}$ such that for any $N \in \mathbb{N}$ and any $\mathbf{x}^1, \dots, \mathbf{x}^N \in \mathcal{X}$, $(Z_{\mathbf{x}^1}, \dots, Z_{\mathbf{x}^N})^\top$ follows a multivariate Gaussian distribution [41]. GPs are fully characterized by their mean function $\mu(\cdot)$ and covariance kernel $k(\cdot, \cdot)$, which are defined as

$$\mu: \mathcal{X} \mapsto \mathbb{R}; \quad \mu(\mathbf{x}) = \mathbb{E}[Z_{\mathbf{x}}] \quad (1)$$

$$k: \mathcal{X} \times \mathcal{X} \mapsto \mathbb{R}; \quad k(\mathbf{x}, \mathbf{x}') = \text{Cov}(Z_{\mathbf{x}}, Z_{\mathbf{x}'}). \quad (2)$$

The mean function reflects our prior belief about the form of f . That is why $\mu(\cdot)$ is also called “prior” mean within the Bayesian framework. While $\mu(\cdot)$ could be any function, $k(\cdot, \cdot)$ must be symmetric positive definite. The most commonly used kernel is the squared exponential (SE) which has the form

$$k(\mathbf{x}, \mathbf{x}') = \sigma^2 \prod_{l=1}^d \exp\left(-\frac{|x_l - x'_l|^2}{2\theta_l^2}\right). \quad (3)$$

In the above equation, the parameter σ^2 , referred to as the *process variance*, controls the scale of the amplitude of sample paths. The parameter θ_l is called the *characteristic length-scale* and controls the degree of smoothness of sample paths along the coordinate l , $1 \leq l \leq d$. Usually the kernel parameters are unknown and need to be estimated. Choosing appropriate kernel parameters has a huge impact on the accuracy of emulators. Cross validation or maximum likelihood estimation are common methods for this purpose.

Covariance kernels play an important role in GP modelling. They customize the structure of sample paths of GPs. As an example, three different kernels (exponential, Matérn 3/2, and SE, see [41] for more information) and the associated sample paths are illustrated in Fig. 1. While in a process incorporating the SE kernel the sample paths are smooth (infinitely differentiable), they are only continuous (not differentiable) when the exponential kernel is used. Herein, we consider *stationary* covariance kernels that are translation invariant. The value of a stationary kernel depends only on the difference between input vectors. In other words, $k(\mathbf{x}, \mathbf{x}') = k(\mathbf{x} + \mathbf{h}, \mathbf{x}' + \mathbf{h})$ for any $\mathbf{h} \in \mathbb{R}^d$.

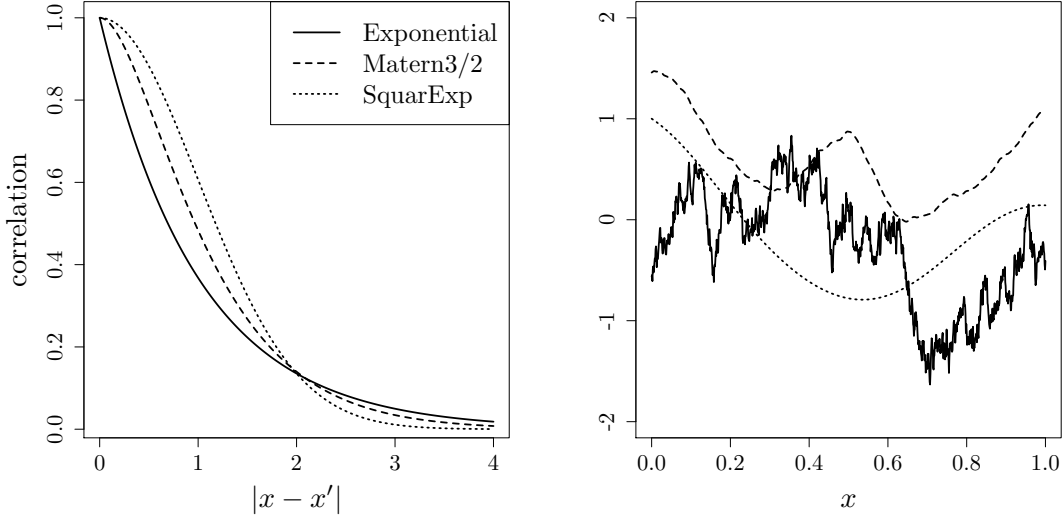


Figure 1: The structure of GP sample paths is determined by the covariance kernel. Left: Graphs of three (stationary) kernels: exponential (solid), Matérn 3/2 (dashed), and squared exponential (dotted). Right: Three sample paths corresponding to the covariance kernels shown on the left picture. The process with squared exponential kernel is infinitely differentiable, whilst with Matérn 3/2 the process is only once differentiable. The process with exponential kernel is not differentiable.

To fit a GP, the true function f is evaluated at n locations $\mathbf{X}_n = \{\mathbf{x}^1, \dots, \mathbf{x}^n\}$ with the corresponding outputs (observations) $\mathbf{y} = (f(\mathbf{x}^1), \dots, f(\mathbf{x}^n))^\top$. Together, \mathbf{X}_n and \mathbf{y} form the set of *training* samples/data denoted by $D = \{\mathbf{X}_n, \mathbf{y}\}$. Then the conditional distribution of $Z_{\mathbf{x}}$ is calculated as:

$\{Z_{\mathbf{x}} \mid D : Z_{\mathbf{x}^1} = f(\mathbf{x}^1), \dots, Z_{\mathbf{x}^n} = f(\mathbf{x}^n)\}$. If the mean function $\mu(\cdot)$ is known, the prediction (conditional mean, $m(\cdot)$) and its uncertainty (conditional variance, $s^2(\cdot)$) at a generic location \mathbf{x}^* are of the form

$$m(\mathbf{x}^*) = \mu(\mathbf{x}^*) + \mathbf{k}(\mathbf{x}^*)^\top \mathbf{K}^{-1} (\mathbf{y} - \mu(\mathbf{X}_n)) \quad (4)$$

$$s^2(\mathbf{x}^*) = k(\mathbf{x}^*, \mathbf{x}^*) - \mathbf{k}(\mathbf{x}^*)^\top \mathbf{K}^{-1} \mathbf{k}(\mathbf{x}^*), \quad (5)$$

where $\mathbf{k}(\mathbf{x}^*) = (k(\mathbf{x}^*, \mathbf{x}^i))_{1 \leq i \leq n}$ is the vector of covariances between the observation at \mathbf{x}^* and the outputs at the \mathbf{x}^i 's and $\mathbf{K} = (k(\mathbf{x}^i, \mathbf{x}^j))_{1 \leq i, j \leq n}$ denotes the matrix of covariances between sample outputs. Also, $\mu(\mathbf{X}_n)$ is the vector of mean function values at the training samples. The mean predictor obtained by Eq. (4) interpolates the points in the training data. Moreover, the prediction uncertainty vanishes at the training points and grows as we get further from them. An illustrative example is shown in Fig. 2.

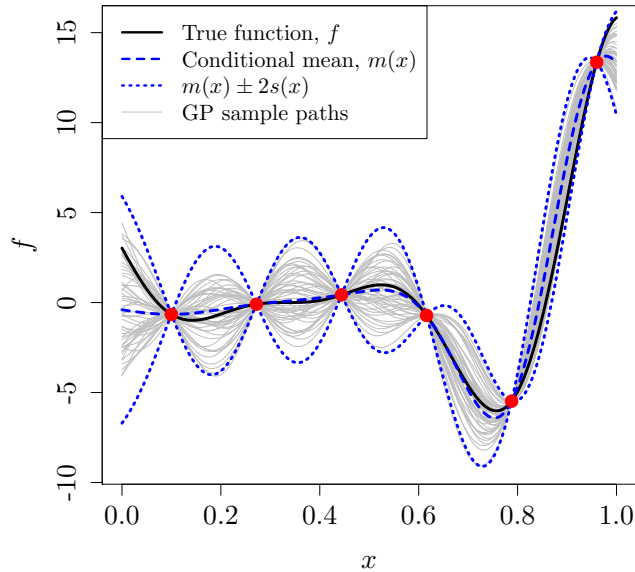


Figure 2: Gaussian process mean (thick dashed blue line) conditional on 6 training samples (red bullets), which is also known as the conditional mean (denoted by $m(x)$), along with confidence intervals (thick dotted blue lines) equal to $m(x) \pm 2s(x)$. True function is the thick solid line. The thin lines are 50 sample paths of the GP.

3 Emulating dynamical simulators

There are many different proposed approaches for emulating dynamic simulators. According to [44], these approaches can be divided into four categories:

1. One method is to use a multi-output emulator for predicting time series output [9]. In this case, the dimension of output space is $q = T$ where T is the length of time the simulator is run for. But when T is large, the efficiency will reduce or may cause numerical problems. In addition, prediction is possible only for a fixed time horizon and one needs to repeat the prediction procedure for different time horizons.

Building q separate emulators for each time point has the drawback of losing some information as the correlation between various outputs (which we expect to be high) is not considered. To take into account such correlation, one can employ multivariate emulators [14, 45], which use nonseparable covariance kernels. However, multivariate emulators are not efficient when the simulator's output is highly multivariate. A common approach to alleviate this problem is to perform dimension reduction techniques on the output space such as principal components analysis [16] and wavelet decomposition [3]. A potential drawback of these techniques is that we may lose some information by leaving out some components.

2. A second approach is to treat time as an additional model input [23]. This method is

computationally demanding as the size of the covariance matrix (see Eqs. (4) and (5)) is nT because the inputs are now $\mathbf{X}_n \times \{1, \dots, T\}$ [9]. Inversion of an $n \times n$ covariance matrix has a computation cost of $\mathcal{O}(n^3)$. Moreover, it is shown in [9] that the performance of multi-output emulators exceeds emulators with time as an extra input.

3. One-step ahead emulations are another example in which the basic assumption is that the model output at a given time depends only on the previous output in time. Then, the transition function needs to be approximated. This method is reported to be efficient, [8].
4. Finally, methods have been described that combine stochastic dynamic models with innovation terms in the form of GPs. For example, in [30] a time-varying auto regression time series, which is a type of dynamic linear model, combined with GPs is used to emulate a dynamic computer code in a hydrological system. Similar work is carried out in [56] with application to climate models.

Here, we propose a methodology based on iterative one-step ahead predictions. We assume that simulating a long time series from the system is expensive. To overcome this, our strategy is to only simulate a short period of time, and to use this simulation to build an emulator that can rapidly approximate longer time simulations. Our method is similar to the work in [8]. However, we propose a methodology to propagate uncertainty through the time series including both the uncertainty of inputs to the emulators at time t and the correlation between them. This is an important aspect of one-step ahead predictions because input to the GP model is uncertain after the first emulation. Besides, it can be used as a criterion to estimate the predictability horizon of an emulator.

3.1 Methodology

We focus on a d -dimensional system of ordinary differential equations (ODEs) of which the state variable is given by the real-valued vector $\mathbf{x}(t) = (x_1(t), \dots, x_d(t))^T$ that we wish to predict over time. This system gives rise to the flow map $\Phi : \mathbb{R}^d \times \mathbb{R} \mapsto \mathbb{R}^d$ which maps $\mathbf{x}(t_0)$ to the solution of the system at time $t \geq t_0$: $\mathbf{x}(t) = \Phi(\mathbf{x}(t_0), t)$. To emulate $\mathbf{x}(t)$, we begin by writing $\Phi(\cdot)$ in d components denoted by f_1, \dots, f_d such that each f_l maps $\mathbf{x}(t_0)$ to $x_l(t)$:

$$\begin{aligned} \Phi(\cdot) &:= (f_1(\cdot), \dots, f_d(\cdot))^T, \\ f_l : \mathbb{R}^d &\mapsto \mathbb{R}; x_l(t) = f_l(\mathbf{x}(t_0)), 1 \leq l \leq d. \end{aligned} \quad (6)$$

In this work, we use a variable order method to integrate the system to $t = t_1, \dots, t_T$ to provide the next step ahead. More precisely, we use the LSODA (Livermore solver for ordinary differential equations with automatic switching between stiff and nonstiff methods) method [38], as implemented in the R package `deSolve`. Then, each function f_l , $1 \leq l \leq d$, is treated as a black-box function maps that $\mathbf{x}(t_0)$ to $x_l(t_1)$. In the next step, f_l s are replaced with their GP emulators denoted by \hat{f}_l s which are iteratively used for one-step ahead predictions over the time horizon T . These instructions are summarized in Algorithm 1.

Note that in Algorithm 1, only the initial input to the emulators is certain. Thereafter, inputs are actually outputs of the emulators in the previous step. For example, to predict \mathbf{x} at t_2 , the

Algorithm 1 Emulation of dynamic non-linear computer models

- 1: Select n samples of initial conditions: $\mathbf{X}_n = \{\mathbf{x}^1(t_0), \dots, \mathbf{x}^n(t_0)\}$
- 2: Run the simulator to obtain $\{\mathbf{x}^1(t_1), \dots, \mathbf{x}^n(t_1)\}$
- 3: **for** $l = 1$ to d **do**
- 4: $\mathbf{y} \leftarrow (x_l^1(t_1), \dots, x_l^n(t_1))^\top$
- 5: Build the l th emulator \hat{f}_l , based on $D = \{\mathbf{X}_n, \mathbf{y}\}$
- 6: **end for**
- 7: Predict over time horizon T given initial condition $\mathbf{x}^*(t_0)$ as follow

$$\begin{aligned}\hat{\mathbf{x}}^*(t_1) &= (\hat{f}_1(\mathbf{x}^*(t_0)), \dots, \hat{f}_d(\mathbf{x}^*(t_0)))^\top \\ \hat{\mathbf{x}}^*(t_2) &= (\hat{f}_1(\hat{\mathbf{x}}^*(t_1)), \dots, \hat{f}_d(\hat{\mathbf{x}}^*(t_1)))^\top \\ &\vdots \\ \hat{\mathbf{x}}^*(t_T) &= (\hat{f}_1(\hat{\mathbf{x}}^*(t_{T-1})), \dots, \hat{f}_d(\hat{\mathbf{x}}^*(t_{T-1})))^\top\end{aligned}$$

input is $\hat{\mathbf{x}}^*(t_1) = (\hat{f}_1(\mathbf{x}^*(t_0)), \dots, \hat{f}_d(\mathbf{x}^*(t_0)))^\top$ in which $\hat{f}_l(\mathbf{x}^*(t_0)) \sim \mathcal{N}(m_l(\mathbf{x}^*(t_0)), s_l^2(\mathbf{x}^*(t_0)))$, $1 \leq l \leq d$, see Eqs. (4) and (5). So, we need to incorporate the input uncertainty in our modelling. The following section deals with this issue.

3.2 Emulation with uncertain input

GPs with uncertain inputs have been studied in [15], [5, 27]. Suppose we want to predict $f(\mathbf{x})$ at random point \mathbf{x}^* drawn from a distribution that has mean μ^* and variance Σ^* . The probability distribution of the prediction at \mathbf{x}^* with the GP emulator \hat{f} is determined by

$$p(\hat{f}(\mathbf{x}^*) | \mu^*, \Sigma^*, D) = \int p(\hat{f}(\mathbf{x}^*) | \mathbf{x}^*, D) p(\mathbf{x}^*) d\mathbf{x}^*. \quad (7)$$

The above integral is analytically intractable [15]. However, it can be approximated using a Monte Carlo (MC) method which relies on samples repeatedly drawn from a probability distribution and statistical analysis to infer the results [43], as demonstrated by an illustrative example in Fig. 3.

An alternative approach is to compute the first and second moments of $p(\hat{f}(\mathbf{x}^*))$ using the law of iterated expectations and conditional variance. If $\hat{f}(\mathbf{x}) \sim \mathcal{N}(m(\mathbf{x}), s^2(\mathbf{x}))$, the mean and variance of $\hat{f}(\mathbf{x}^*)$, assuming \mathbf{x}^* has the normal distribution, are given by

$$\mathbb{E}[\hat{f}(\mathbf{x}^*) | \mu^*, \Sigma^*] = \mathbb{E}_{\mathbf{x}^*} \left[\mathbb{E}_{\hat{f}(\mathbf{x}^*)} [\hat{f}(\mathbf{x}^*) | \mathbf{x}^*] \right] = \mathbb{E}_{\mathbf{x}^*} [m(\mathbf{x}^*)] \quad (8)$$

$$\begin{aligned}\text{Var}[\hat{f}(\mathbf{x}^*) | \mu^*, \Sigma^*] &= \mathbb{E}_{\mathbf{x}^*} \left[\text{Var}_{\hat{f}(\mathbf{x}^*)} [\hat{f}(\mathbf{x}^*) | \mathbf{x}^*] \right] + \text{Var}_{\mathbf{x}^*} \left[\mathbb{E}_{\hat{f}(\mathbf{x}^*)} [\hat{f}(\mathbf{x}^*) | \mathbf{x}^*] \right] \\ &= \mathbb{E}_{\mathbf{x}^*} [s^2(\mathbf{x}^*)] + \text{Var}_{\mathbf{x}^*} [m(\mathbf{x}^*)].\end{aligned} \quad (9)$$

Still, computing quantities in (8) and (9) is not straightforward because they are functions of the random variable \mathbf{x}^* . One can approximate $m(\mathbf{x}^*)$ and $s^2(\mathbf{x}^*)$ using a Taylor expansion around

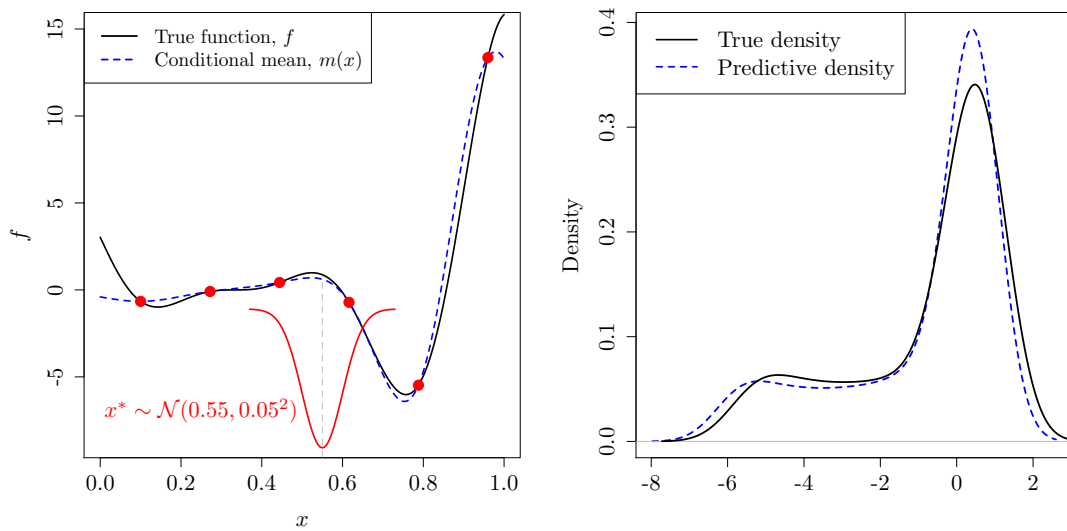


Figure 3: Estimating probability distribution of the output given the distribution of the inputs using the Monte Carlo method. Left: the model input is uncertain with the probability distribution: $x^* \sim \mathcal{N}(0.55, 0.05^2)$, as shown by the red line. Right: the estimated output distributions for the true function (solid) and the emulator (dashed blue). These estimates are based on $n_{MC} = 10000$ samples drawn from x^* that are propagated in $f(\cdot)$ and $m(\cdot)$. Performing such a large number of function evaluations is impractical if f is computationally expensive.

μ^* , first order for the former and second order for the latter. They are given by [5]:

$$m(\mathbf{x}^*) = m(\mu^*) + \left. \frac{\partial m(\mathbf{x}^*)}{\partial \mathbf{x}^*} \right|_{\mathbf{x}^*=\mu^*}^\top (\mathbf{x}^* - \mu^*) + O(\|\mathbf{x}^* - \mu^*\|^2) \quad (10)$$

$$s^2(\mathbf{x}^*) = s^2(\mu^*) + \left. \frac{\partial s^2(\mathbf{x}^*)}{\partial \mathbf{x}^*} \right|_{\mathbf{x}^*=\mu^*}^\top (\mathbf{x}^* - \mu^*) + \frac{1}{2} (\mathbf{x}^* - \mu^*)^\top \left. \frac{\partial^2 s^2(\mathbf{x}^*)}{\partial \mathbf{x}^* \partial \mathbf{x}^{*\top}} \right|_{\mathbf{x}^*=\mu^*} (\mathbf{x}^* - \mu^*) + O(\|\mathbf{x}^* - \mu^*\|^3). \quad (11)$$

Rewriting Eqs. (8) and (9) based on the first and the second order Taylor expansions leads to [15]

$$\mathbb{E} [\hat{f}(\mathbf{x}^*) | \mu^*, \Sigma^*] \approx \mathbb{E}_{\mathbf{x}^*} \left[m(\mu^*) + \left. \frac{\partial m(\mathbf{x}^*)}{\partial \mathbf{x}^*} \right|_{\mathbf{x}^*=\mu^*}^\top (\mathbf{x}^* - \mu^*) \right] = m(\mu^*) \quad (12)$$

$$\begin{aligned} \text{Var} [\hat{f}(\mathbf{x}^*) | \mu^*, \Sigma^*] &\approx s^2(\mu^*) + \frac{1}{2} \text{Tr} \left\{ \left. \frac{\partial^2 s^2(\mathbf{x}^*)}{\partial \mathbf{x}^* \partial \mathbf{x}^{*\top}} \right|_{\mathbf{x}^*=\mu^*} \Sigma^* \right\} \\ &+ \left. \frac{\partial m(\mathbf{x}^*)}{\partial \mathbf{x}^*} \right|_{\mathbf{x}^*=\mu^*}^\top \Sigma^* \left. \frac{\partial m(\mathbf{x}^*)}{\partial \mathbf{x}^*} \right|_{\mathbf{x}^*=\mu^*}, \end{aligned} \quad (13)$$

where Tr is the trace operator. Derivatives of the conditional mean and the variance in Eqs. (12) and (13) can be calculated analytically. For detailed information, we refer the reader to [34]. It is also possible to use the MC method. For example, to approximate $\mathbb{E}_{\mathbf{x}^*} [m(\mathbf{x}^*)]$ in Eq. (8), samples are repeatedly drawn from the random variable \mathbf{x}^* . Then, they are propagated through the function $m(\cdot)$ defined in Eq. (4). Finally, the desired quantity is approximated using

$$\mathbb{E}_{\mathbf{x}^*} [m(\mathbf{x}^*)] \approx \frac{1}{n_{MC}} \sum_{i=1}^{n_{MC}} m(\mathbf{x}^{*i}), \quad (14)$$

where n_{MC} denotes the number of MC samples.

4 One-step ahead predictions with uncertain inputs

In this section we first describe the emulator which is applied for predicting dynamic models. We then examine the prediction capability of the emulator on two well studied dynamical systems: the Lorenz and the Van der Pol systems, which are described in subsequent sections.

The GP emulator we use in our experiments consists of a first order polynomial regression for the mean function in Eq. (1) (i.e., $\mu(\mathbf{x}) = \beta_0 + \beta_1 \mathbf{x}$) and a squared exponential kernel, given in Eq. (3), for the covariance kernel k . These choices of μ and k are recommended in [8]. A set of training samples of size $n = 12d$, as recommended in [20, 31], is drawn over the space of initial conditions. Our training sample is constrained to lie in a cube. For example, a suitable boundary for the Lorenz attractor, as described in [1, 55], is given by the unstable manifold of the origin. To define a bounding box that contains the attractor, we therefore simulated the

system with initial conditions close to the origin and chose as boundaries in each coordinate the extremes of the simulation. Note we do assume that the system is constrained to lie in the same volume, although clearly we would like to capture most of the variation. The points should be selected based on a space-filling sampling scheme, and we therefore use a Latin hypercube [51, 39]. The goal in a space-filling design is to spread the points *evenly* within the input space. No attempt is made to have the points lie along the stable manifold, we simply try to ‘fill’ space.

To build each emulator \hat{f}_l ($1 \leq l \leq d$), the training data consists of $\mathbf{X} = \{\mathbf{x}^1(t_0), \dots, \mathbf{x}^n(t_0)\}$ with the corresponding outputs $\mathbf{y} = (x_l^1(t_1), \dots, x_l^n(t_1))^\top$. The R packages `DiceKriging` [46] and `deSolve` [50] are employed to fit the GP emulator and to solve differential equations, respectively. The unknown parameters of the SE kernel k (i.e. σ and θ 's) and the mean function μ (i.e. β_0 and β_1) are estimated by maximum likelihood implemented in `DiceKriging`. To solve ODEs, we use the default solver of `deSolve`, called “ode”, which is based on the LSODA method [38]. A full Jacobian matrix is used which is calculated internally by LSODA. The error control (the relative and absolute tolerances) performed by the solver is 10^{-6} . In these two examples, we use a time step equal to 0.01, i.e. $t_{v+1} - t_v = 0.01$, $\forall v \in \{1, 2, \dots, T-1\}$.

4.1 Lorenz system

The Lorenz model was first proposed by Edward Lorenz in 1963 [32] as a mathematical representation of atmospheric convection. It is a three-dimensional system of ordinary differential equations. Under certain choices of parameters it can display chaotic behaviour, i.e. its behaviour is highly sensitive to initial conditions. The evolution of three state variables is described by [50]

$$\begin{cases} \frac{dx_1}{dt} = ax_1 + x_2x_3 \\ \frac{dx_2}{dt} = b(x_2 - x_3) \\ \frac{dx_3}{dt} = -x_1x_2 + cx_2 - x_3, \end{cases} \quad (15)$$

where a , b and c are parameters [53]. Here, we assume $a = -8/3$, $b = -10$ and $c = 28$. We focus on the case with initial conditions $\mathbf{x}(t_0) = (x_1(t_0) = 1, x_2(t_0) = 1, x_3(t_0) = 1)^\top$. To propagate input uncertainty, we have implemented two alternative methods, Taylor expansion and Monte Carlo, to approximate Eqs. (8) and (9). Since they yield similar results, for the sake of brevity, we only present emulations obtained using the MC approach.

Emulation of the Lorenz model using the iterative one-step ahead predictions considering the input uncertainty, as described in Algorithm 1, is demonstrated in Fig. 4. We show the evolution of predictions for each system variable over time, as well as a three-dimensional picture showing the evolution of the whole system, $(x_1(t), x_2(t), x_3(t))$. The solid line represents the true model and the dashed blue line is the GP prediction. It can be seen that the prediction precision is high at the beginning of the time course, for example $t \leq 14$. However, the emulator deviates from the true model as time progresses. Fig. 4 suggests that the emulator is well suited to describing the evolution of the system within a “wing” of the Lorenz attractor, but that predictions break down upon switching to the other part of the attractor.

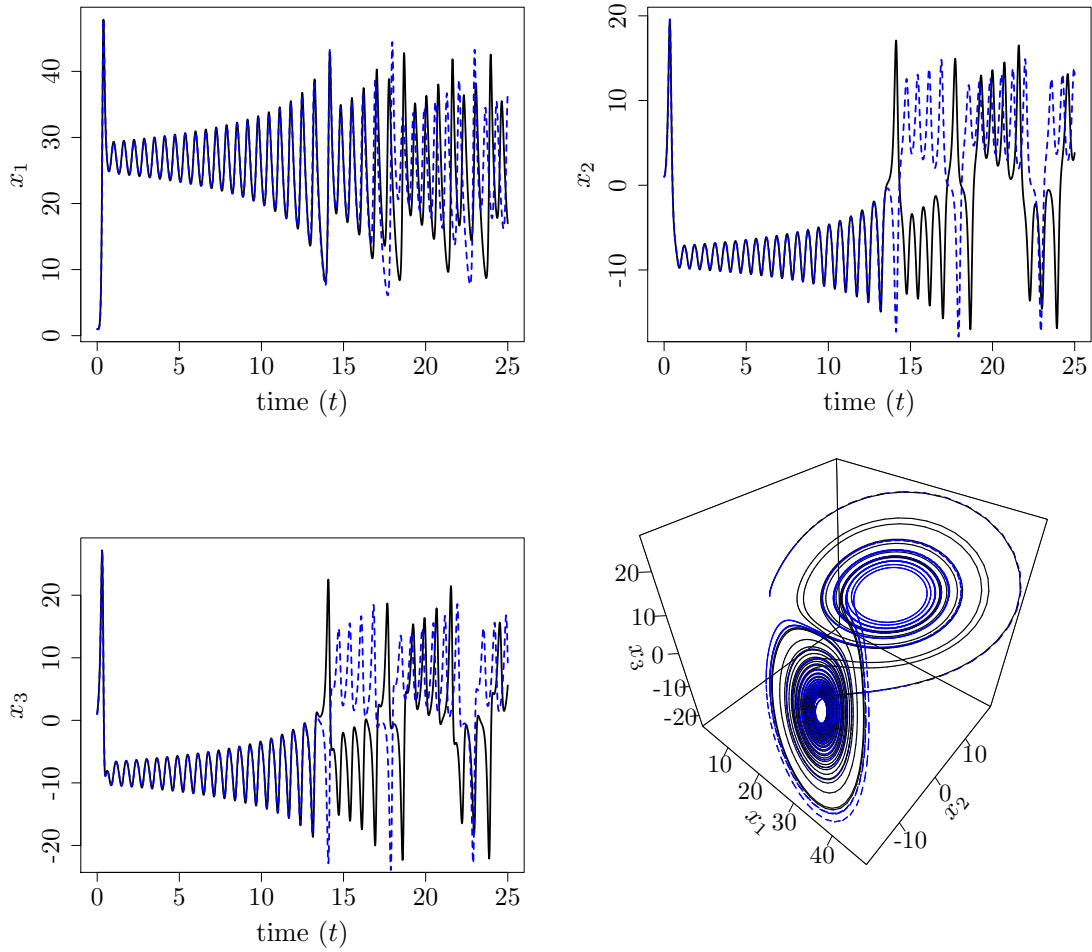


Figure 4: Lorenz system (solid black) and its emulation (dashed blue). The 1-D pictures illustrate evolution of state variables x_1, x_2, x_3 and their predictions. The emulators built based on iterative one-step ahead predictions are able to well predict up to about $t = 14$. The 3-D picture shows the evolution and prediction of the whole system.

Fig. 5 shows the uncertainties (solid black) associated with the predictions illustrated in Fig. 4. The uncertainties are compared with the case in which the input uncertainty is not considered (dashed red line). Generally, if emulation is carried out with uncertain inputs, the order of uncertainties is higher. Nevertheless, they are still too small and contrary to our expectations do not increase with time as the uncertainty builds up from step to step. The true model is not inside the credible intervals, which are defined as $m(\mathbf{x}^*) \pm 2s(\mathbf{x}^*)$. Note the credible intervals are not shown on Fig. 4, but can easily be derived from Figs. 4 and 5. In particular, we would expect the uncertainty to “blow up” when we reach the bifurcation point (at about $t=14$) where our emulator can be on a different branch to the true model but still has very small uncertainty.

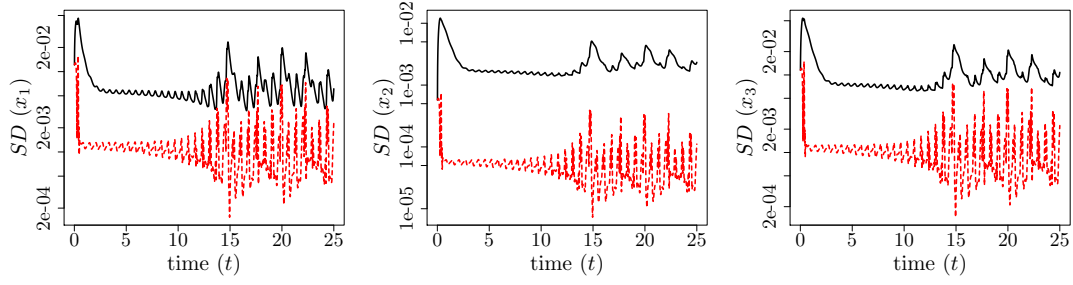


Figure 5: Standard deviation (SD) associated with the predictions of state variables of Lorenz system (Fig. 4) with and without considering input uncertainty, solid black and dashed red lines respectively. Incorporating input uncertainty augments the prediction SD. Contrary to our expectations, the uncertainties do not grow with time.

4.2 Van der Pol oscillator

The Van der Pol model was first introduced by the Dutch electrical engineer Balthasar van der Pol in 1920. The Van der Pol oscillator models express the behaviour of nonlinear vacuum tube circuits. In its two-dimensional form, it is given by the following ordinary differential equations [53]

$$\begin{cases} \frac{dx_1}{dt} = x_2 \\ \frac{dx_2}{dt} = \alpha(1 - x_1^2)x_2 - x_1. \end{cases} \quad (16)$$

Here, the scalar $\alpha > 0$ determines the nonlinearity and the strength of damping.

The results of predicting state variables of the Van der Pol oscillator is illustrated in Fig. 6. The corresponding uncertainties are given by Fig. 7. The initial condition is $\mathbf{x}(t_0) = (x_1 = 1, x_2 = 1)^\top$ and $\alpha = 5$. The difference between emulation and the true model is indistinguishable up to about $t = 100$. Again, considering the input uncertainty augments prediction uncertainties everywhere. But, since they are small, the true model is not inside the credible intervals when prediction accuracy declines. In the next section, we propose a method to better propagate uncertainty.

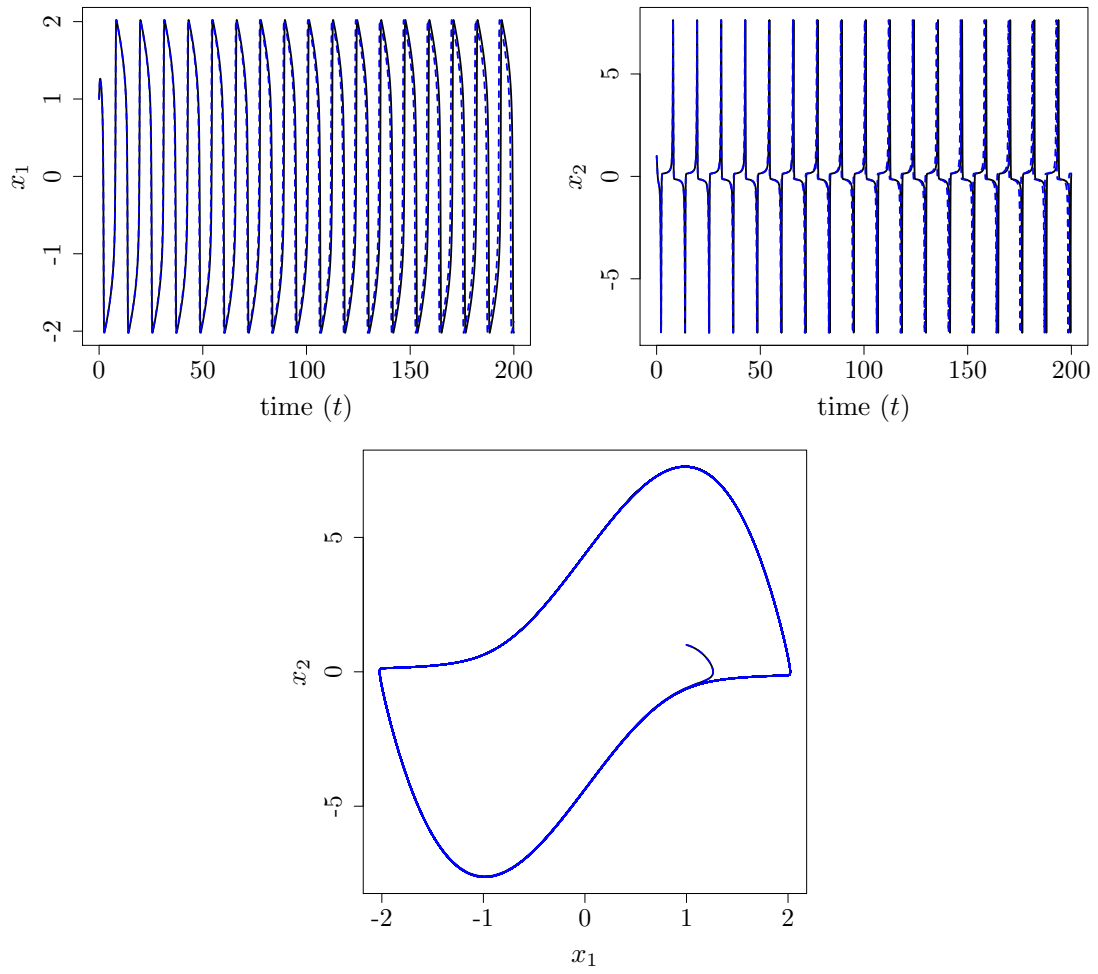


Figure 6: Top: Evolution of state variables of the Van der Pol oscillator (solid black) and their predictions (dashed blue). The prediction capability of emulators remains high even if the simulation continues until $t = 200$. Bottom: Evolution and prediction of state variables together.

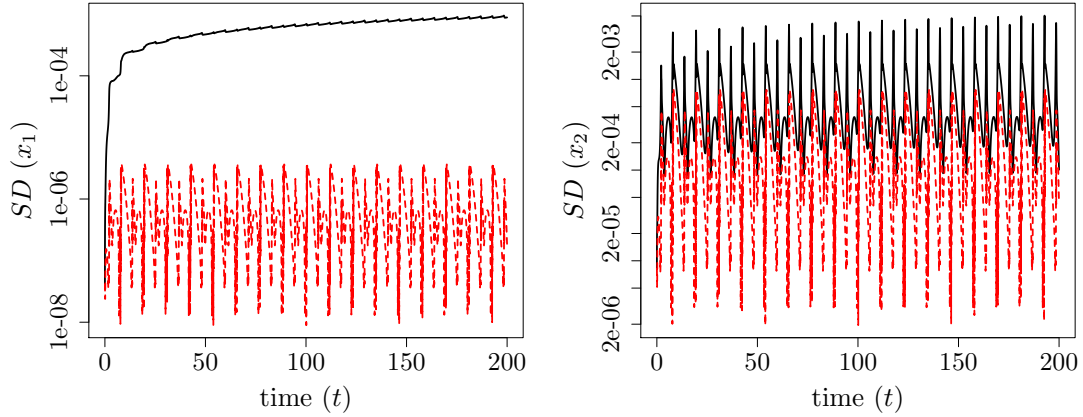


Figure 7: Standard deviation (SD) of predicting Van der Pol with and without considering input uncertainty, solid black and dashed red lines respectively.

5 Propagating the uncertainty

In the previous section, each element of $\mathbf{x}(t) = (x_1(t), x_2(t), \dots, x_d(t))^\top$ is emulated separately; d different GP emulators denoted by $\hat{f}_1, \hat{f}_2, \dots, \hat{f}_d$ are employed independently such that the l -th emulator \hat{f}_l emulates the transition function f_l defined as $f_l : \mathbf{x}(t_0) \mapsto x_l(t_1)$. However, we may lose some information if correlation between emulators is neglected. As we will see later, this is the reason why uncertainties are small and do not grow with time.

Let $\mathbf{x}^* \sim \mathcal{N}(\boldsymbol{\mu}^*, \boldsymbol{\Sigma}^*)$ be an uncertain input to the d emulators. As a result, $\mathbf{x}^{**} = (\hat{f}_1(\mathbf{x}^*), \dots, \hat{f}_d(\mathbf{x}^*))^\top$ is a random vector whose mean is determined by

$$\boldsymbol{\mu}^{**} = (\mathbb{E}[\hat{f}_1(\mathbf{x}^*)|\boldsymbol{\mu}^*, \boldsymbol{\Sigma}^*], \dots, \mathbb{E}[\hat{f}_d(\mathbf{x}^*)|\boldsymbol{\mu}^*, \boldsymbol{\Sigma}^*])^\top.$$

Notice that \mathbf{x}^{**} is not necessarily a random normal variable, see Fig. 3. But, we approximate its distribution by a Gaussian. Let $\boldsymbol{\Sigma}^{**}$ be the covariance matrix of \mathbf{x}^{**} . In order to include the correlation between emulators, $\boldsymbol{\Sigma}^{**}$ must be of the form:

$$\begin{bmatrix} \text{Var}[\hat{f}_1(\mathbf{x}^*)|\boldsymbol{\mu}^*, \boldsymbol{\Sigma}^*] & \dots & \text{Cov}[\hat{f}_1(\mathbf{x}^*), \hat{f}_d(\mathbf{x}^*)|\boldsymbol{\mu}^*, \boldsymbol{\Sigma}^*] \\ \vdots & \ddots & \vdots \\ \text{Cov}[\hat{f}_d(\mathbf{x}^*), \hat{f}_1(\mathbf{x}^*)|\boldsymbol{\mu}^*, \boldsymbol{\Sigma}^*] & \dots & \text{Var}[\hat{f}_d(\mathbf{x}^*)|\boldsymbol{\mu}^*, \boldsymbol{\Sigma}^*] \end{bmatrix}.$$

The diagonal elements of $\boldsymbol{\Sigma}^{**}$ are calculated using Eq. (9) which is approximated by the MC method. The off-diagonal elements, i.e. cross covariances, are given by:

$$\begin{aligned} \text{Cov}[\hat{f}_l(\mathbf{x}^*), \hat{f}_j(\mathbf{x}^*)|\boldsymbol{\mu}^*, \boldsymbol{\Sigma}^*] &= \mathbb{E}[\hat{f}_l(\mathbf{x}^*)\hat{f}_j(\mathbf{x}^*)|\boldsymbol{\mu}^*, \boldsymbol{\Sigma}^*] \\ &- \mathbb{E}[\hat{f}_l(\mathbf{x}^*)|\boldsymbol{\mu}^*, \boldsymbol{\Sigma}^*] \mathbb{E}[\hat{f}_j(\mathbf{x}^*)|\boldsymbol{\mu}^*, \boldsymbol{\Sigma}^*], \quad 1 \leq l, j \leq d, l \neq j. \end{aligned} \quad (17)$$

The cross covariances can be obtained analytically when the kernel is the squared exponential, see [34]. Herein, we use the MC method to approximate the cross covariances in Eq.

(17):

$$\begin{aligned} \text{Cov} [\hat{f}_1(\mathbf{x}^*), \hat{f}_j(\mathbf{x}^*) | \mu^*, \Sigma^*] &\approx \frac{1}{n_{MC}} \sum_{i=1}^{n_{MC}} \hat{f}_1(\mathbf{x}^{*i}) \hat{f}_j(\mathbf{x}^{*i}) \\ &- \left(\frac{1}{n_{MC}} \sum_{i=1}^{n_{MC}} \hat{f}_1(\mathbf{x}^{*i}) \right) \left(\frac{1}{n_{MC}} \sum_{i=1}^{n_{MC}} \hat{f}_j(\mathbf{x}^{*i}) \right). \end{aligned} \quad (18)$$

To shed more light on this method, we present here the mean and the covariance matrix of the input in one-step ahead predictions:

- at $t = 0$, the input is deterministic,

$$\mathbf{x}^*(t_0) \sim \mathcal{N} \left(\mathbf{x}^*(t_0), \begin{bmatrix} 0 & \dots & 0 \\ \vdots & \vdots & \vdots \\ 0 & \dots & 0 \end{bmatrix} \right)$$

- at $t = 1$,

$$\hat{\mathbf{x}}^*(t_1) \sim \mathcal{N} \left(\begin{bmatrix} \mathbb{E} [\hat{f}_1(\mathbf{x}^*(t_0))] \\ \vdots \\ \mathbb{E} [\hat{f}_d(\mathbf{x}^*(t_0))] \end{bmatrix}, \begin{bmatrix} \text{Var} [\hat{f}_1(\mathbf{x}^*(t_0))] & \dots & 0 \\ \vdots & \vdots & \vdots \\ 0 & \dots & \text{Var} [\hat{f}_d(\mathbf{x}^*(t_0))] \end{bmatrix} \right)$$

- at $t = 2$, the input to emulators are no longer deterministic and the method described in this section should be applied,

$$\hat{\mathbf{x}}^*(t_2) \stackrel{app.}{\sim} \mathcal{N} \left(\begin{bmatrix} \mathbb{E} [\hat{f}_1(\hat{\mathbf{x}}^*(t_1))] \\ \vdots \\ \mathbb{E} [\hat{f}_d(\hat{\mathbf{x}}^*(t_1))] \end{bmatrix}, \begin{bmatrix} \text{Var} [\hat{f}_1(\hat{\mathbf{x}}^*(t_1))] & \dots & \text{Cov} [\hat{f}_1(\hat{\mathbf{x}}^*(t_1)), \hat{f}_d(\hat{\mathbf{x}}^*(t_1))] \\ \vdots & \vdots & \vdots \\ \text{Cov} [\hat{f}_d(\hat{\mathbf{x}}^*(t_1)), \hat{f}_1(\hat{\mathbf{x}}^*(t_1))] & \dots & \text{Var} [\hat{f}_d(\hat{\mathbf{x}}^*(t_1))] \end{bmatrix} \right)$$

⋮

- at $t = T$,

$$\hat{\mathbf{x}}^*(t_T) \stackrel{app.}{\sim} \mathcal{N} \left(\begin{bmatrix} \mathbb{E} [\hat{f}_1(\hat{\mathbf{x}}^*(t_{n-1}))] \\ \vdots \\ \mathbb{E} [\hat{f}_d(\hat{\mathbf{x}}^*(t_{n-1}))] \end{bmatrix}, \begin{bmatrix} \text{Var} [\hat{f}_1(\hat{\mathbf{x}}^*(t_{n-1}))] & \dots & \text{Cov} [\hat{f}_1(\hat{\mathbf{x}}^*(t_{n-1})), \hat{f}_d(\hat{\mathbf{x}}^*(t_{n-1}))] \\ \vdots & \vdots & \vdots \\ \text{Cov} [\hat{f}_d(\hat{\mathbf{x}}^*(t_{n-1})), \hat{f}_1(\hat{\mathbf{x}}^*(t_{n-1}))] & \dots & \text{Var} [\hat{f}_d(\hat{\mathbf{x}}^*(t_{n-1}))] \end{bmatrix} \right)$$

The results of emulating the Lorenz and Van der Pol models considering input uncertainties together with the correlation between emulators are illustrated in Figs. 8 and 9, respectively. The predictive capability of these emulators is high at the beginning of the time course, say up to $t = 25$, and tends to the average of the system afterwards (dashed blue lines). In the case of the Lorenz model, the true model predominantly remains inside the credible intervals (= prediction $\pm 2 \times$ prediction standard deviation). The uncertainty grows and reaches its maximum, interestingly, when deviation from the true model begins. From this point onwards the expected

value of the emulator is the long term average of the underlying function and the uncertainty is large enough to encompass most values of the system. We interpret this as the emulator in effect “giving up” on trying to emulate the value at a particular time t and instead falling back on a prediction for a random time. Such a prediction is useless in practice but statistically makes sense. This point can be used as a measure for the *predictability horizon* of dynamic emulators which is illustrated in Fig. 10. The picture on the left of Fig. 10 is associated with prediction uncertainties of variables in the Lorenz system while that on the right shows variables of the Van der Pol model. The y -axis in Fig. 10 is on logarithmic scale.

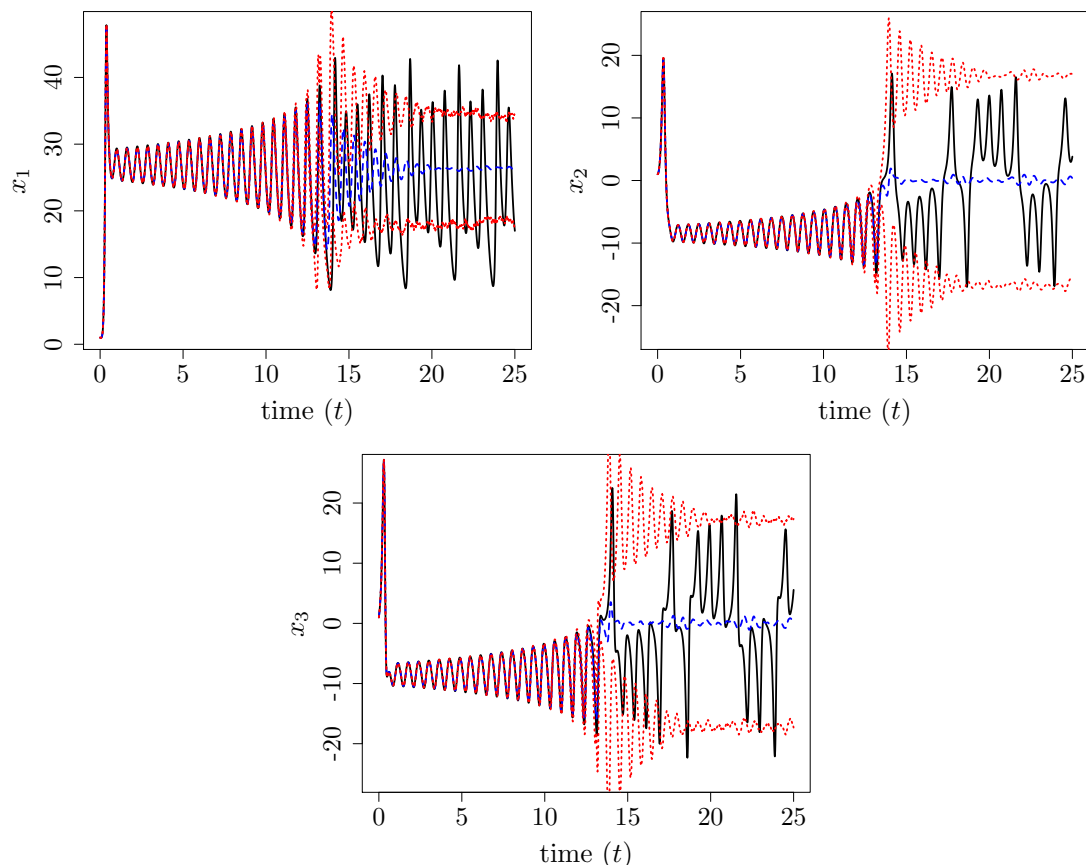


Figure 8: Emulating the Lorenz system (solid black) considering input uncertainties and the correlation between emulators. The prediction (dashed blue) tends to the average of the process when the emulator is not able to predict the true model well, up to $t = 14$. However, the credible intervals (dotted red) are large enough to contain the true model most of the time. Note the prediction uncertainty reaches its maximum around $t = 14$ where deviation from the true model occurs.

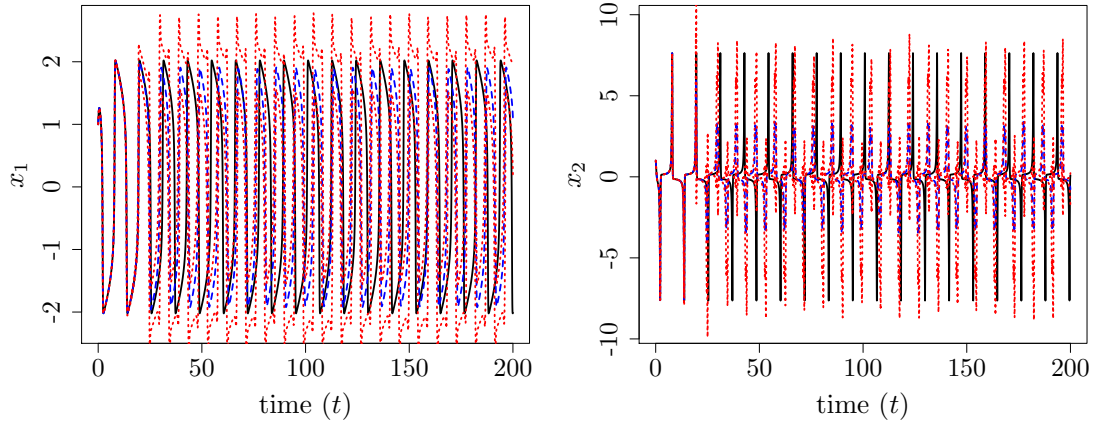


Figure 9: Emulating the Van der Pol model (solid black) considering input uncertainties and the correlation between emulators. The predictive capability of the emulator (dashed blue) is high at the beginning of the time course, up to approximately $t = 25$, but subsequently is a frequency miss-match and the prediction damps. However, the maximum of prediction uncertainties (dotted red) occurs at approximately $t = 25$ which indicates deviation of emulator from the true model.

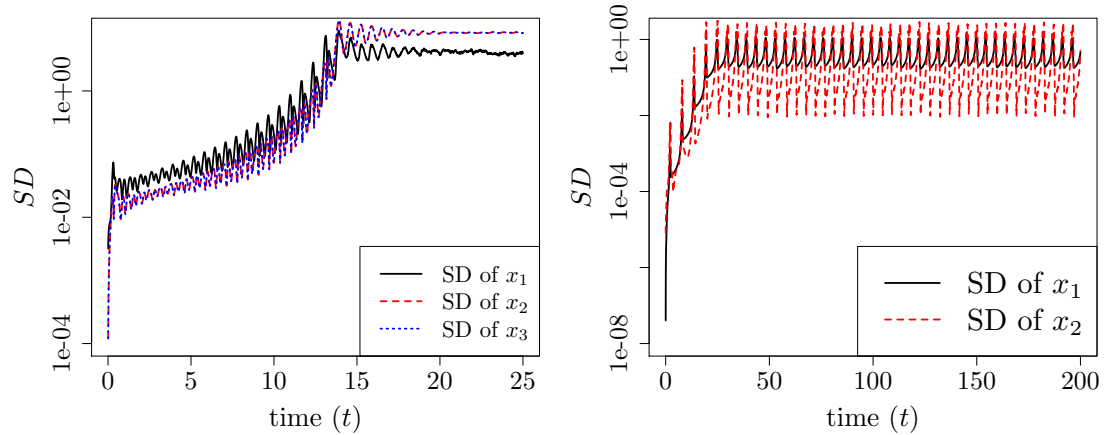


Figure 10: Left: standard deviation (SD) of prediction associated with the three variables in the Lorenz model. Right: SD of prediction associated with the two variables in the Van der Pol model. The y-axis is on logarithmic scale. In both cases, an SD reaches its maximum where the corresponding emulator can not well predict the true model. This can be used as an criterion to detect the predictability horizon of dynamic emulators.

We now propose an alternative approach to emulate dynamic models. In this method, correlations between emulators are not considered in prediction. However, they are incorporated for uncertainty propagation. At each step, the prediction and the associated uncertainty are obtained based on different inputs denoted by \mathbf{x}_P^* and \mathbf{x}_{SD}^* , respectively. To better illustrate this approach,

the emulation procedure at $t = 2$ and 3 is given below. Note that $\mathbf{x}_p^* = \mathbf{x}_{SD}^*$ up to time $t = 2$.

- at $t = 2$

$$\hat{\mathbf{x}}_p^*(t_2) \stackrel{app.}{\sim} \mathcal{N} \left(\begin{bmatrix} \mathbb{E} [\hat{f}_1(\hat{\mathbf{x}}^*(t_1))] \\ \vdots \\ \mathbb{E} [\hat{f}_d(\hat{\mathbf{x}}^*(t_1))] \end{bmatrix}, \begin{bmatrix} \text{Var} [\hat{f}_1(\hat{\mathbf{x}}^*(t_1))] & \dots & 0 \\ \vdots & \ddots & \vdots \\ 0 & \dots & \text{Var} [\hat{f}_d(\hat{\mathbf{x}}^*(t_1))] \end{bmatrix} \right)$$

$$\hat{\mathbf{x}}_{SD}^*(t_2) \stackrel{app.}{\sim} \mathcal{N} \left(\begin{bmatrix} \mathbb{E} [\hat{f}_1(\hat{\mathbf{x}}^*(t_1))] \\ \vdots \\ \mathbb{E} [\hat{f}_d(\hat{\mathbf{x}}^*(t_1))] \end{bmatrix}, \begin{bmatrix} \text{Var} [\hat{f}_1(\hat{\mathbf{x}}^*(t_1))] & \dots & \text{Cov} [\hat{f}_1(\hat{\mathbf{x}}^*(t_1)), \hat{f}_d(\hat{\mathbf{x}}^*(t_1))] \\ \vdots & \ddots & \vdots \\ \text{Cov} [\hat{f}_d(\hat{\mathbf{x}}^*(t_1)), \hat{f}_1(\hat{\mathbf{x}}^*(t_1))] & \dots & \text{Var} [\hat{f}_d(\hat{\mathbf{x}}^*(t_1))] \end{bmatrix} \right)$$

- at $t = 3$

$$\hat{\mathbf{x}}^*(t_3) \stackrel{app.}{\sim} \mathcal{N} \left(\begin{bmatrix} \mathbb{E} [\hat{f}_1(\hat{\mathbf{x}}_p^*(t_2))] \\ \vdots \\ \mathbb{E} [\hat{f}_d(\hat{\mathbf{x}}_p^*(t_2))] \end{bmatrix}, \begin{bmatrix} \text{Var} [\hat{f}_1(\hat{\mathbf{x}}_{SD}^*(t_2))] & \dots & \text{Cov} [\hat{f}_1(\hat{\mathbf{x}}_{SD}^*(t_2)), \hat{f}_d(\hat{\mathbf{x}}_{SD}^*(t_2))] \\ \vdots & \ddots & \vdots \\ \text{Cov} [\hat{f}_d(\hat{\mathbf{x}}_{SD}^*(t_2)), \hat{f}_1(\hat{\mathbf{x}}_{SD}^*(t_2))] & \dots & \text{Var} [\hat{f}_d(\hat{\mathbf{x}}_{SD}^*(t_2))] \end{bmatrix} \right)$$

$$\hat{\mathbf{x}}_p^*(t_3) \stackrel{app.}{\sim} \mathcal{N} \left(\begin{bmatrix} \mathbb{E} [\hat{f}_1(\hat{\mathbf{x}}_p^*(t_2))] \\ \vdots \\ \mathbb{E} [\hat{f}_d(\hat{\mathbf{x}}_p^*(t_2))] \end{bmatrix}, \begin{bmatrix} \text{Var} [\hat{f}_1(\hat{\mathbf{x}}_p^*(t_2))] & \dots & 0 \\ \vdots & \ddots & \vdots \\ 0 & \dots & \text{Var} [\hat{f}_d(\hat{\mathbf{x}}_p^*(t_2))] \end{bmatrix} \right)$$

$$\hat{\mathbf{x}}_{SD}^*(t_3) \stackrel{app.}{\sim} \mathcal{N} \left(\begin{bmatrix} \mathbb{E} [\hat{f}_1(\hat{\mathbf{x}}_{SD}^*(t_2))] \\ \vdots \\ \mathbb{E} [\hat{f}_d(\hat{\mathbf{x}}_{SD}^*(t_2))] \end{bmatrix}, \begin{bmatrix} \text{Var} [\hat{f}_1(\hat{\mathbf{x}}_{SD}^*(t_2))] & \dots & \text{Cov} [\hat{f}_1(\hat{\mathbf{x}}_{SD}^*(t_2)), \hat{f}_d(\hat{\mathbf{x}}_{SD}^*(t_2))] \\ \vdots & \ddots & \vdots \\ \text{Cov} [\hat{f}_d(\hat{\mathbf{x}}_{SD}^*(t_2)), \hat{f}_1(\hat{\mathbf{x}}_{SD}^*(t_2))] & \dots & \text{Var} [\hat{f}_d(\hat{\mathbf{x}}_{SD}^*(t_2))] \end{bmatrix} \right)$$

The predictive capability of this approach is illustrated in Figs. 11 and 12. The results are in line with this approach being a combination of emulation with uncertain inputs and the method explained earlier this section. As can be seen, predictions in this case do not tend to the time-series mean once the discrepancy between the emulator and the true model increases, which occurs when the prediction uncertainty reaches its maximum. Rather, the emulator persists in approximating trajectories on the attractor. However, this method could be relatively time-consuming because prediction and uncertainty of prediction are calculated separately.

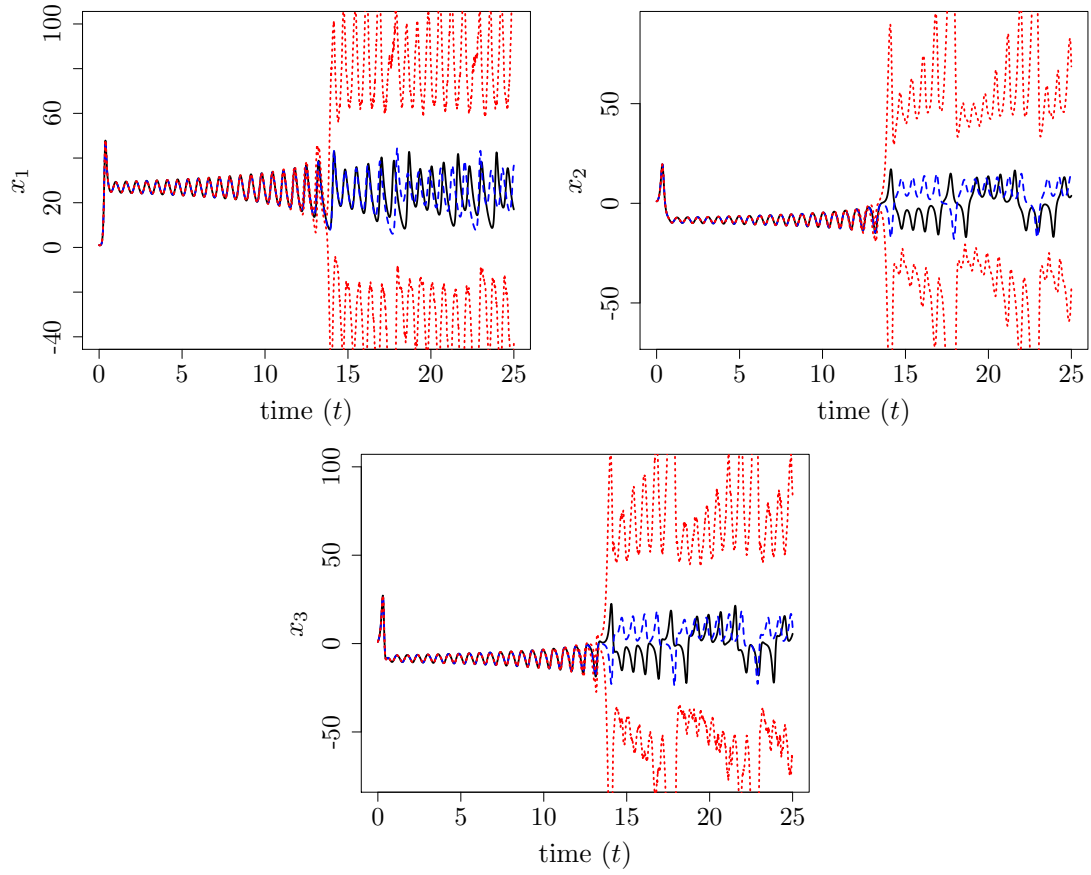


Figure 11: Emulating the Lorenz system (solid black): prediction (dashed blue) and the credible intervals (dotted red). Correlations between emulators are not considered in prediction (\mathbf{x}_P^* is used as input to emulators) while they are incorporated in uncertainty estimation (\mathbf{x}_{SD}^* is used as input to emulators).

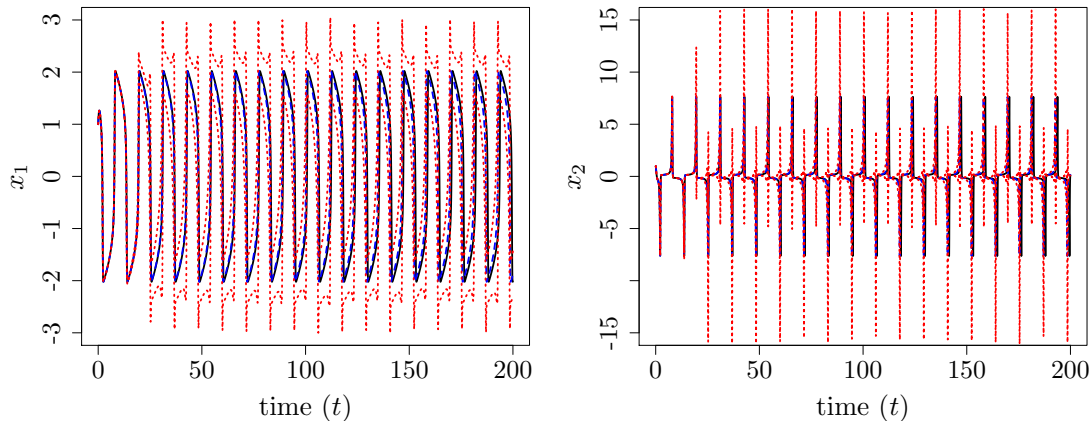


Figure 12: Emulating the Van der Pol model (solid black): prediction (dashed blue) and the credible intervals (dotted red).

6 Conclusion

In this paper we develop a general framework to emulate dynamically highly non-linear functions with time series outputs using Gaussian processes. Such functions show the behaviour of phenomena evolving with time. One advantage of our method is that it is easy to implement in comparison to alternative methods; it uses a GP emulator to perform one-step ahead predictions in an iterative way over the whole time series. Moreover, we propose a number of ways to propagate uncertainty through the time series based on both the uncertainty of inputs to the emulators and the correlation between them. This allows to measure the horizon, we term the “predictability horizon”, within which the prediction accuracy is high. The capability of our method is illustrated in application to two non-linear dynamical systems: the Lorenz and Van der Pol systems. In both cases, we obtained a very good predictive performance and an accurate measure of the predictability horizon.

Acknowledgements

The authors gratefully acknowledge the financial support of the EPSRC via grant EP/N014391/1. We warmly thank Jennifer Creaser for the constructive discussions.

References

- [1] V. S. Afraimovich, V. V. Bykov, and L. P. Shilnikov. On the origin and structure of the Lorenz attractor. *Akademiia Nauk SSSR Doklady*, 234:336–339, 1977.
- [2] C.A.L. Bailer-Jones, T. J. Sabin, D. J. C. Mackay, and P.J. Withers. Prediction of deformed and annealed microstructures using Bayesian neural networks and Gaussian processes. In

Proceedings of the Australasia Pacific Forum on Intelligent Processing and Manufacturing of Materials, pages 913–919, 1997.

- [3] M. J. Bayarri, J. O. Berger, J. Cafeo, G. Garcia-Donato, F. Liu, J. Palomo, R. J. Parthasarathy, R. Paulo, J. Sacks, and D. Walsh. Computer model validation with functional output. *The Annals of Statistics*, 35(5):1874–1906, 2007.
- [4] P.J. Birrell, G. Ketsetzis, N.J. Gay, B.S. Cooper, A.M. Presanis, R.J. Harris, A. Charlett, X-S. Zhang, P.J. White, R.G. Pebody, and Angelis D. De. Bayesian modeling to unmask and predict influenza A/H1N1 pdm dynamics in London. *Proceedings of the national academy of sciences of The United States of America*, 108:18238–18243, 2011.
- [5] Joaquin Quiñonero Candela, Agathe Girard, Jan Larsen, and Carl Edward Rasmussen. Propagation of uncertainty in Bayesian kernel models - application to multiple-step ahead forecasting. In *International Conference on Acoustics, Speech and Signal Processing*, pages 701–704. IEEE, 2003.
- [6] Peter Challenor. The probability of rapid climate change. *Significance*, 1(4):155–158, 2004.
- [7] Victoria C. P. Chen, Kwok-Leung Tsui, Russell R. Barton, and Martin Meckesheimer. A review on design, modeling and applications of computer experiments. *IIE Transactions*, 38(4):273–291, 2006.
- [8] S. Conti, J. P. Gosling, J. E. Oakley, and A. O’Hagan. Gaussian process emulation of dynamic computer codes. *Biometrika*, 96:663–676, September 2009.
- [9] Stefano Conti and Anthony O’Hagan. Bayesian emulation of complex multi-output and dynamic computer models. *Journal of Statistical Planning and Inference*, 140(3):640–651, 2010.
- [10] N.A.C. Cressie. *Statistics for spatial data*. Wiley series in probability and mathematical statistics: Applied probability and statistics. J. Wiley, 1993.
- [11] Marian Farah, Paul Birrell, Stefano Conti, and Daniela De Angelis. Bayesian emulation and calibration of a dynamic epidemic model for A/H1N1 influenza. *Journal of the American Statistical Association*, 109(508):1398–1411, 2014.
- [12] Lauric A. Ferrat, Marc Goodfellow, and John R. Terry. Classifying dynamic transitions in high dimensional neural mass models: A random forest approach. *PLOS Computational Biology*, 14(3):1–27, 03 2018.
- [13] Alexander I.J. Forrester and Andy J. Keane. Recent advances in surrogate-based optimization. *Progress in Aerospace Sciences*, 45(1-3):50 – 79, 2009.
- [14] Thomas E. Fricker, Jeremy E. Oakley, and Nathan M. Urban. Multivariate Gaussian process emulators with nonseparable covariance structures. *Technometrics*, 55(1):47–56, 2013.

- [15] Agathe Girard, Carl Edward Rasmussen, Joaquin Quiñonero Candela, and Roderick Murray-Smith. Gaussian process priors with uncertain inputs - application to multiple-step ahead time series forecasting. In *Advances in Neural Information Processing Systems 15*, pages 545–552. MIT Press, 2003.
- [16] Dave Higdon, James Gattiker, Brian Williams, and Maria Rightley. Computer model calibration using high-dimensional output. *Journal of the American Statistical Association*, 103(482):570–583, 2008.
- [17] Ruichen Jin, Wei Chen, and Timothy W. Simpson. Comparative studies of metamodeling techniques under multiple modeling criteria. *Structural and Multidisciplinary Optimization*, 23:1–13, 2000.
- [18] Ruichen Jin, Wei Chen, and Agus Sudjianto. On sequential sampling for global metamodeling in engineering design. In *Design Engineering Technical Conferences And Computers and Information in Engineering*, volume 2, pages 539–548, 2002.
- [19] Bradley Jones and Rachel T. Johnson. Design and analysis for the Gaussian process model. *Quality and Reliability Engineering International*, 25:515–524, 2009.
- [20] Donald R. Jones, Matthias Schonlau, and William J. Welch. Efficient global optimization of expensive black-box functions. *Journal of Global Optimization*, 13(4):455–492, 1998.
- [21] Alfredo A. Kalaitzis and title="A Simple Approach to Ranking Differentially Expressed Gene Expression Time Courses through Gaussian Process Regression Lawrence, Neil D.". *BMC Bioinformatics*, 12(1):180, 2011.
- [22] Aditya Kamath, Rodrigo A. Vargas-Hernandez, Roman V. Krems, Tucker Carrington, and Sergei Manzhos. Neural networks vs Gaussian process regression for representing potential energy surfaces: A comparative study of fit quality and vibrational spectrum accuracy. *The Journal of Chemical Physics*, 148(24):241702, 2018.
- [23] Marc C. Kennedy and Anthony O’Hagan. Bayesian calibration of computer models. *Journal of the Royal Statistical Society: Series B (Statistical Methodology)*, 63(3):425–464, 2001.
- [24] Jack P.C. Kleijnen. Kriging metamodeling in simulation: A review. *European Journal of Operational Research*, 192(3):707 – 716, 2009.
- [25] Andreas Krause, Ajit Singh, and Carlos Guestrin. Near-optimal sensor placements in Gaussian processes: Theory, efficient algorithms and empirical studies. *Journal of Machine Learning Research*, 9:235–284, February 2008.
- [26] George Kuczera, Dmitri Kavetski, Stewart Franks, and Mark Thyer. Towards a Bayesian total error analysis of conceptual rainfall-runoff models: Characterising model error using storm-dependent parameters. *Journal of Hydrology*, 331(1):161 – 177, 2006.

- [27] Malte Kuß. *Gaussian process models for robust regression, classification, and reinforcement learning*. PhD thesis, Technische Universität Darmstadt, Darmstadt, Germany, Darmstadt, April 2006.
- [28] Neil Lawrence, Guido Sanguinetti, and Magnus Rattray. Modelling transcriptional regulation using Gaussian Processes. In *NIPS 2006*, 2006.
- [29] L. A. Lee, K. S. Carslaw, K. J. Pringle, G. W. Mann, and D. V. Spracklen. Emulation of a complex global aerosol model to quantify sensitivity to uncertain parameters. *Atmospheric Chemistry and Physics*, 11(23):12253–12273, 2011.
- [30] F. Liu and M. West. A dynamic modelling strategy for Bayesian computer model emulation. *Bayesian Analysis*, 4(2):393–412, 2009.
- [31] Jason L. Loepky, Jerome Sacks, and William J. Welch. Choosing the sample size of a computer experiment: A practical guide. *Technometrics*, 51(4):366–376, 2009.
- [32] Edward N. Lorenz. Deterministic nonperiodic flow. *Journal of Atmospheric Sciences*, 20:130–148, 1963.
- [33] D. J. C. MacKay. Introduction to Gaussian processes. In C. M. Bishop, editor, *Neural Networks and Machine Learning*, pages 133–166. Springer-Verlag, 1998.
- [34] Andrew McHutchon. *Nonlinear modelling and control using Gaussian processes*. PhD thesis, University of Cambridge UK, Department of Engineering, 2014.
- [35] Radford M. Neal. *Bayesian Learning for Neural Networks*. Lecture Notes in Statistics. Springer-Verlag New York, 1996.
- [36] Radford M. Neal. Regression and classification using Gaussian process priors. pages 475–501. *Bayesian Statistics 6*, Oxford University Press, 1998.
- [37] A. O’Hagan. Bayesian analysis of computer code outputs: A tutorial. *Reliability Engineering & System Safety*, 91(10-11):1290–1300, 2006.
- [38] Linda Petzold. Automatic selection of methods for solving stiff and nonstiff systems of ordinary differential equations. *SIAM Journal on Scientific and Statistical Computing*, 4(1):136–148, 1983.
- [39] Luc Pronzato and Werner G. Müller. Design of computer experiments: space filling and beyond. *Statistics and Computing*, 22(3):681–701, 2012.
- [40] Carl Edward Rasmussen. *Evaluation of Gaussian processes and other methods for non-linear regression*. PhD thesis, Toronto, Ont., Canada, Canada, 1997.
- [41] Carl Edward Rasmussen and Christopher K. I. Williams. *Gaussian processes for machine learning (adaptive computation and machine learning)*. The MIT Press, 2005.

- [42] J.O. Rawlings, S.G. Pantula, and D.A. Dickey. *Applied Regression Analysis: A Research Tool*. Springer Texts in Statistics. Springer New York, 2006.
- [43] Samik Raychaudhuri. Introduction to Monte Carlo simulation. In *Proceedings of the 40th Conference on Winter Simulation*, pages 91–100, 2008.
- [44] P. Reichert, G. White, Maria J. Bayarri, and E. Bruce Pitman. Mechanism-based emulation of dynamic simulation models: Concept and application in hydrology. *Computational Statistics & Data Analysis*, 55(4):1638–1655, 2011.
- [45] Jonathan Rougier. Efficient emulators for multivariate deterministic functions. *Journal of Computational and Graphical Statistics*, 17(4):827–843, 2008.
- [46] Olivier Roustant, David Ginsbourger, and Yves Deville. DiceKriging, DiceOptim: Two R packages for the analysis of computer experiments by kriging-based metamodeling and optimization. *Journal of Statistical Software*, 51(1):1–55, 2012.
- [47] Jerome Sacks, William J. Welch, Toby J. Mitchell, and Henry P. Wynn. Design and analysis of computer experiments. *Statistical Science*, 4(4):409–423, 1989.
- [48] T. J. Santner, Williams B., and Notz W. *The design and analysis of computer experiments*. Springer-Verlag, 2003.
- [49] A. Schwaighofer, M. Grigoras, V. Tresp, and C. Hoffmann. *GPPS: A Gaussian process positioning system for cellular networks*. Number 16 in Advances in Neural Information Processing Sys. MIT Press, 2004.
- [50] Karlina Soetaert, Thomas Petzoldt, and R. Woodrow Setzer. Solving differential equations in R: Package deSolve. *Journal of Statistical Software*, 33(9):1–25, 2010.
- [51] Michael Stein. Large sample properties of simulations using Latin hypercube sampling. *Technometrics*, 29(2):143–151, 1987.
- [52] H. Stommel. Thermohaline convection with two stable regimes of flow. *Tellus*, 13:224–230, 1961.
- [53] S.H. Strogatz. *Nonlinear dynamics and chaos*. Studies in nonlinearity. Sarat Book House, 2007.
- [54] Peter S. Swain, Keiran Stevenson, Allen Leary, Luis F. Montano-Gutierrez, Ivan B. N. Clark, Jackie Vogel, and Teuta Pilizota. Inferring time derivatives including cell growth rates using Gaussian processes. *Nature Communications*, 7(4):273–291, 2016.
- [55] R. F. Williams. The structure of Lorenz attractors. *Publications Mathematiques de l’Institut des Hautes Etudes Scientifiques*, 50:73–99, 1979.
- [56] Daniel Williamson and Adam T. Blaker. Evolving Bayesian emulators for structured chaotic time series, with application to large climate models. *SIAM/ASA Journal on Uncertainty Quantification*, 2(1):1–28, 2014.